



CdS/Au/Ti/Pb(Mg_{1/3}Nb_{2/3})_{0.7}Ti_{0.3}O₃ photocatalysts and biphotoelectrodes with ferroelectric polarization in single domain for efficient water splitting

Zhimin Song^{a,b}, Bin Hong^a, Xiaodi Zhu^a, Fan Zhang^a, Shikuo Li^b, Jianjun Ding^c, Xiaoming Jiang^d, Jun Bao^{a,**}, Chen Gao^a, Song Sun^{a,b,*}

^a National Synchrotron Radiation Laboratory, Collaborative Innovation Center of Chemistry for Energy Materials, University of Science & Technology of China, Hefei, Anhui 230029, China

^b School of Chemistry and Chemical Engineering, Anhui University, Hefei, Anhui 230601, China

^c Institute of Applied Technology, Hefei Institutes of Physical Science, Chinese Academy of Sciences, Hefei 230031, China

^d Beijing Advanced Sciences and Innovation Center of Chinese Academy of Sciences, Beijing 100083, China



ARTICLE INFO

Keywords:
Photocatalysis
Ferroelectric polarization
CdS
Water splitting
 $\text{Pb}(\text{Mg}_{1/3}\text{Nb}_{2/3})_{0.7}\text{Ti}_{0.3}\text{O}_3$

ABSTRACT

The construction of efficient photocatalysts for water splitting is still challenging, mainly due to the unexpected recombination of photogenerated carriers. Ferroelectric polarization-induced charge separation of photocatalysts has been demonstrated as an effective method for improving photocatalytic performance. However, ferroelectric domains in existing works are random before polarization-switching, which results in lower polarization electric field intensity and limits the charge separation efficiency. Here, we report that the spontaneous ferroelectric polarization in a single domain for efficient charge separation over a representative semiconductor CdS, in the form of CdS/Au/Ti/Pb(Mg_{1/3}Nb_{2/3})_{0.7}Ti_{0.3}O₃ (CdS/Au/Ti/PMN-PT), for water splitting in absence of any cocatalyst or external voltage. The photocurrent value of the positive polarized CdS/Au/Ti/PMN-PT yields 1.70 mA·cm⁻², which is about 20 times higher than the value of the non-polarized sample. In addition, a biphotoelectrode cell composed of a positively and a negatively polarized CdS/Au/Ti/PMN-PT was constructed. A considerable solar-to-hydrogen conversion efficiency of 0.19% was achieved. It was found that the interfacial resistance and the surface reaction kinetics may be the main factors governing the photocatalytic performance. This work not only provides a strategy to promote charge separation but also develops a new biphotoelectrode cell capable of obtaining efficient solar water splitting.

1. Introduction

Photocatalytic water splitting for clean hydrogen generation in an environmentally friendly way has received extensive attention in the field of solar-energy conversion [1–4]. Photocatalysis without an external applied voltage is expected to be the least expensive water splitting approach due to its simplicity and low operation cost [5]. However, existing work is still far from industrial demands of solar-to-hydrogen (STH) conversion efficiency according to the techno-economic evaluation [6,7]. One of the major obstacles is the fast recombination of photogenerated carriers [8,9]. In general, photo-generated charge carriers transfer from bulk to reactive sites requires hundreds of picoseconds and the reaction between charge carriers and adsorbed water molecules on the surface of photocatalysts occurs on a

time scale ranging from nanoseconds to several microseconds. However, the recombination process of photogenerated charge carriers only counts for several picoseconds to dozens of nanoseconds [10,11]. In other words, most of the photogenerated electrons and holes prefer to recombine in the bulk before reaching the photocatalyst surface [12].

To achieve the effective charge separation, numerous strategies have been attempted, including morphology and grain control [13–15], defect engineering [16–18], loading cocatalysts [19,20], and constructing Z-scheme systems [21–23]. In addition, the efficiency of charge separation can be increased by introducing a space charge region in photocatalyst composites, such as building p-n/n-n junction [24,25], phase junction [26,27], dipole moment [28] and aligning the vectors of electric field [29]. As such, the internal electric field with a desirable strength facilitates the suppression of the recombination of

* Corresponding author at: National Synchrotron Radiation Laboratory, Collaborative Innovation Center of Chemistry for Energy Materials, University of Science & Technology of China, Hefei, Anhui 230029, China.

** Corresponding author.

E-mail addresses: baoj@ustc.edu.cn (J. Bao), suns@ustc.edu.cn (S. Sun).

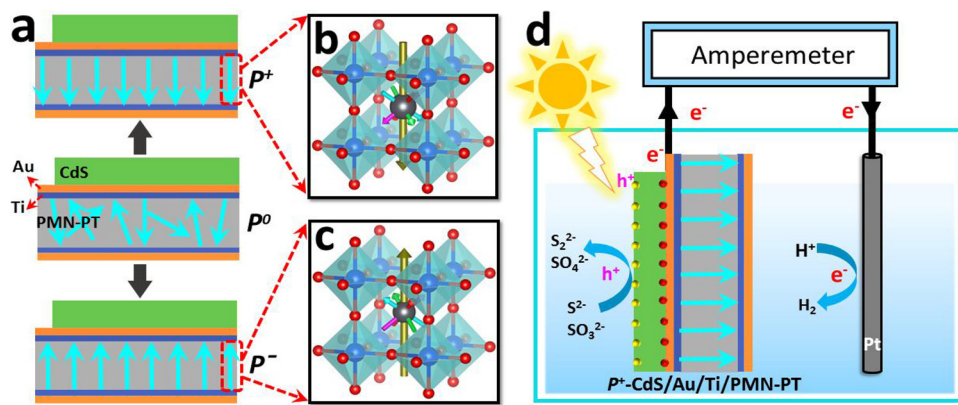


Fig. 1. (a) Scheme of the structures of P° -CdS/Au/Ti/PMN-PT, P^+ -CdS/Au/Ti/PMN-PT, and P^- -CdS/Au/Ti/PMN-PT. The structures of (b) positive and (c) negative polarized PMN-PT in the P^+ -CdS/Au/Ti/PMN-PT, and P^- -CdS/Au/Ti/PMN-PT, respectively. The gray, red, and blue balls represent Pb atoms, O atoms and $(\text{Mg}_{1/3}\text{Nb}_{2/3})_{0.7}\text{Ti}_{0.3}$ units, respectively. (d) Scheme of photocatalytic water splitting over P^+ -CdS/Au/Ti/PMN-PT without external bias (For interpretation of the references to colour in this figure legend, the reader is referred to the web version of this article).

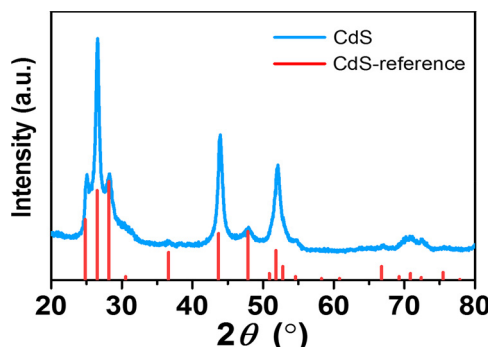


Fig. 2. XRD pattern of the as-prepared CdS powders extracted from the CdS/Au/Ti/PMN-PT, and the reference CdS.

photogenerated carriers [30–32]. As a new method for internal electric field induced charge separation, introducing polarization field of ferroelectric or piezoelectric materials has been demonstrated to be effective for improving catalytic activity on powders or films [33–37]. For instance, Wang et al. [38] reported the photoelectrochemical water splitting was significantly enhanced on TiO₂ nanowires after coating ferroelectric BaTiO₃ shell. Cui et al. [39] found that BaTiO₃/α-Fe₂O₃ hybrid photocatalytic performance enhancement was associated with improved charge-carrier separation at the interface between the ferroelectric surface and the hematite. In addition, Li et al. [40] reported the potential of ferroelectric polarization towards tuning epitaxial growth of TiO₂ photocatalyst. Very recently, ferroelectrics with polar domains has also been utilized to enhance the charge separation of photocatalysts for improving photocatalytic performance in powder suspension [41]. However, in most cases the ferroelectric domains in existing works are random before ferroelectric polarization-switching, which results in lower polarization field intensity and limits the charge separation efficiency in comparison to that with a single domain.

Herein, we introduced a ferroelectric spontaneous polarization electric field (SPE) with a single domain to separate charge carriers on a CdS/Au/Ti/Pb(Mg_{1/3}Nb_{2/3})_{0.7}Ti_{0.3}O₃ photocatalyst for highly efficient water splitting without applying any external voltage or cocatalyst. In this work, the typical ferroelectric Pb(Mg_{1/3}Nb_{2/3})_{0.7}Ti_{0.3}O₃ (PMN-PT) single crystal is used as the SPE layer to generate a nonvolatile polarization field because it exhibits an ultrahigh piezoelectric coefficient d_{33} (the c -axis strain in response to a field along a cube axis c) of $\sim 2500 \text{ pCN}^{-1}$, a large strain level of 1.7%, and low hysteresis, in contrast to the conventional piezoelectric ceramics [42]. Meanwhile, CdS with an absorption edge up to 560 nm is chosen as a model photocatalyst since it has been widely used as an authentic and active H₂ evolution photocatalyst in water splitting in a hole sacrificial reagent circumstance [43–45]. In the configuration of CdS/Au/Ti/PMN-PT, SPE gives full play to the role of the charge separation so that the water splitting is rate-determined by the interfacial resistance and the surface reaction

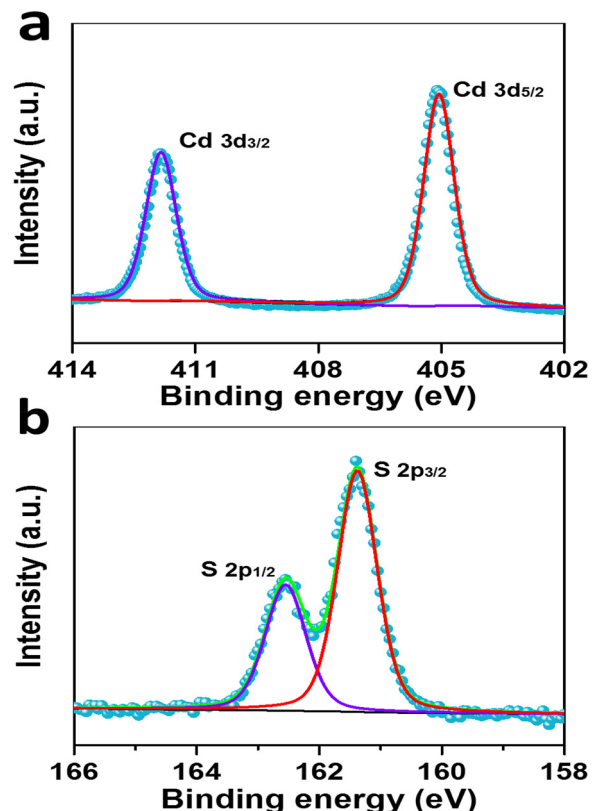


Fig. 3. (a) Cd 3d and (b) S 2p XPS spectra obtained from CdS/Au/Ti/PMN-PT.

kinetics rather than charge separation. The photocurrent value of the positive polarized CdS/Au/Ti/PMN-PT yields 1.70 mA cm^{-2} , which is about 20 times higher than the value of the non-polarized sample. Furthermore, by controlling the polarization directions, a new bi-photoelectrode cell composed of a positively and a negatively polarized photocatalyst can be constructed, and a considerable photocatalytic performance are therefore obtained.

2. Experimental

2.1. Preparation of CdS/Au/Ti/PMN-PT

Firstly, Au/Ti/PMN-PT film was fabricated by the magnetron sputtering method [46,47]. Au/Ti layers were deposited in a LAB 18 magnetron sputtering system (Kurt J. Lesker Company, USA). Prior to the deposition, the base pressure of the magnetron sputtering system was pumped to $1.6 \times 10^{-8} \text{ Torr}$ at least. A Ti layer and Au layer with respective thickness of about 5, and 20 nm were successively deposited on

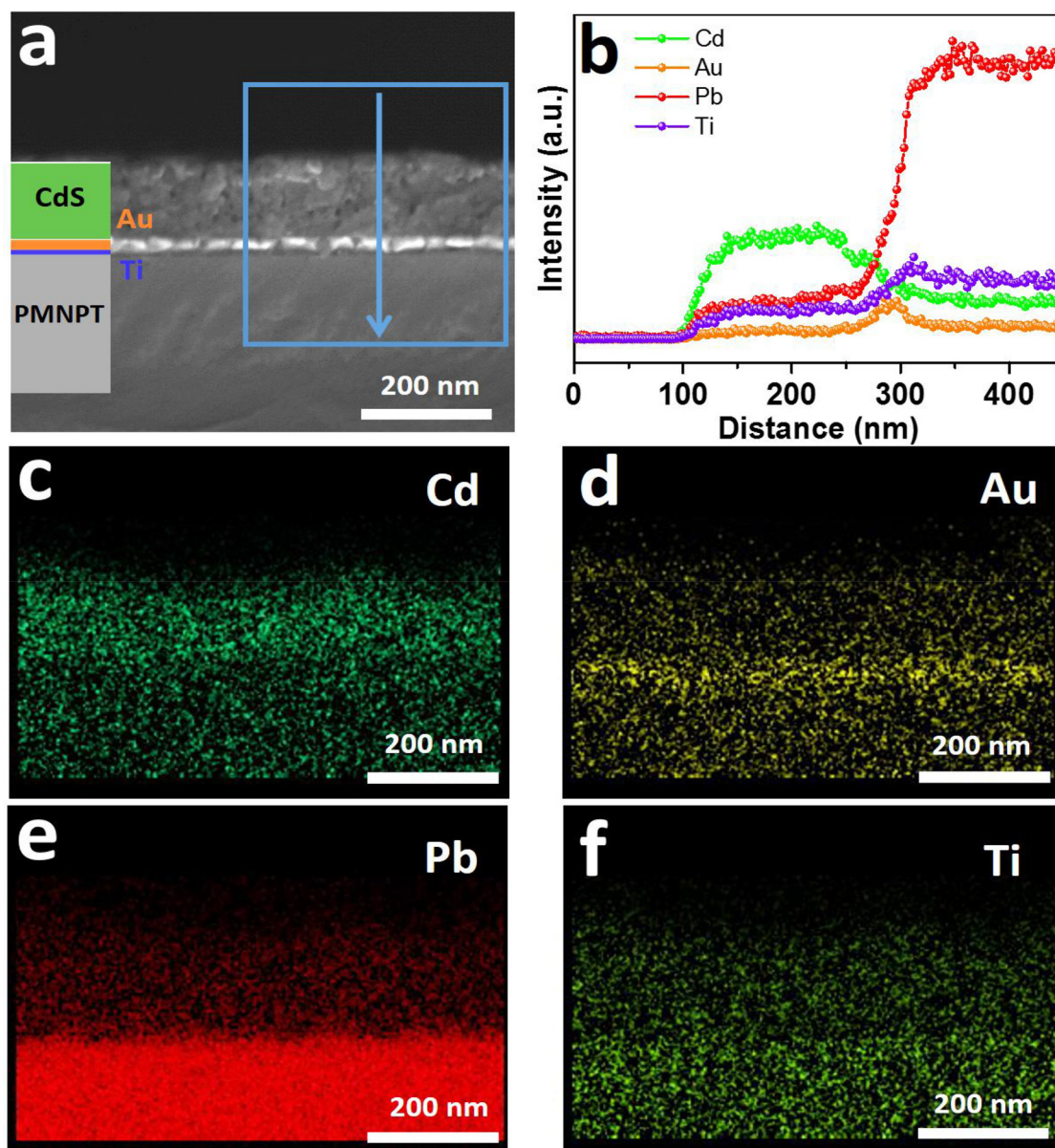


Fig. 4. (a) Cross-sectional SEM image of CdS/Au/Ti/PMN-PT and the corresponding (b) EDX line-scan analyses and (c–f) mapping images for (c) Cd, (d) Au, (e) Pb, and (f) Ti distribution.

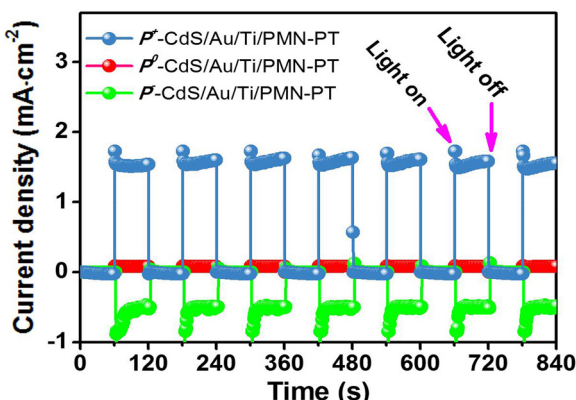


Fig. 5. Chronoamperometric responses for P^+ , P° , and P^- -CdS/Au/Ti/PMN-PT samples under AM 1.5 G simulated sunlight in 0.25 M Na_2S and 0.35 M Na_2SO_3 mixed aqueous solution without applied bias voltage, acquired by Keithley 2410-C source meter.

(001)-oriented PMN-PT ($10 \times 5 \times 0.5 \text{ mm}^3$) single crystalline substrates at room temperature in 3 mTorr argon (Ar) atmosphere. The growth rates of the Ti and Au layers were calibrated to be about 0.4 \AA s^{-1} and 0.2 \AA s^{-1} , respectively. The Ti located between Au and the PMN-PT substrates is used as an adhesive layer for Au layer, while the Au layer was used as a conductive layer.

Subsequently the CdS photocatalyst was grown on the Au/Ti/PMN-PT by a chemical bath method [48,49]. In a typical process, 0.16 g $3\text{CdSO}_4 \cdot 8\text{H}_2\text{O}$ (99.9%, Sinopharm Chemical Reagent Co., Ltd) and 0.84 g $\text{SC}(\text{NH}_2)_2$ (99.9%, Sinopharm Chemical Reagent Co., Ltd) was dissolved into 100 mL deionized water under stirring at room temperature. Then 8.5 mL $\text{NH}_3 \cdot \text{H}_2\text{O}$ (25%–28%, Sinopharm Chemical Reagent Co., Ltd) was added into the above solution with continually stirring, until the solution became a faint yellow color. The as-prepared Au/Ti/PMN-PT film was immersed into the above solution. The solution was heated to 60 °C under stirring, then kept at 60 °C for 7 min. The resulting CdS/Au/Ti/PMN-PT was taken out and washed with deionized water for several times, followed by drying in Ar stream. Finally, the sample was annealed at 400 °C in Ar atmosphere for 1 h with a

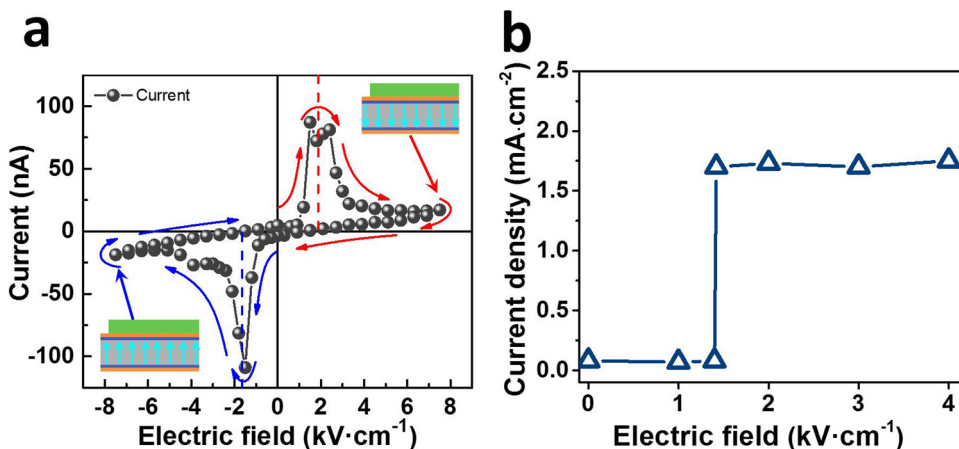


Fig. 6. (a) The polarization-switching induced current vs. voltage curves for the PMN-PT. The sweeping sequence loop is from positive electric field to negative electric field. (b) photocurrent densities of P^+ -CdS/Au/Ti/PMN-PT dependent on the applied voltages for polarization of PMN-PT.

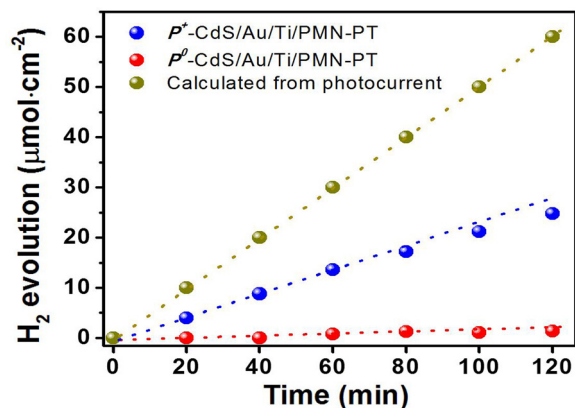


Fig. 7. Time course of H_2 evolution on P^+ -CdS/Au/Ti/PMN-PT and P^0 -CdS/Au/Ti/PMN-PT with a counter Pt electrode without applying external voltage under AM 1.5 G simulated sunlight in $0.25 \text{ M Na}_2\text{S}$ and $0.35 \text{ M Na}_2\text{SO}_3$ mixed aqueous solution. The expected H_2 production calculated from the photocurrent of Fig. 5 is presented as a reference.

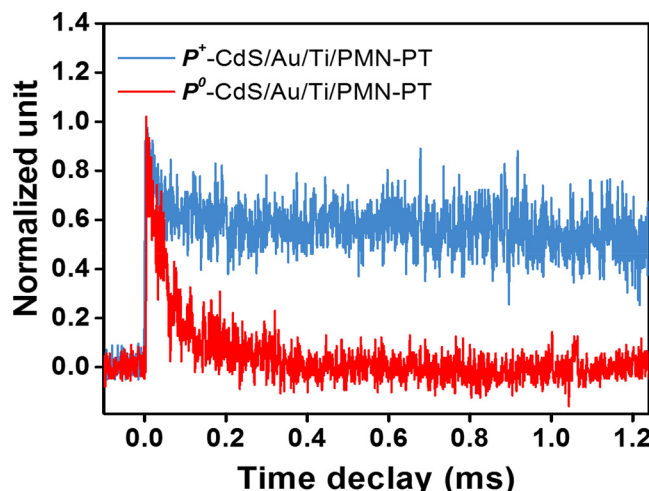


Fig. 8. Normalized transient absorption profiles of P^+ -CdS/Au/Ti/PMN-PT and P^0 -CdS/Au/Ti/PMN-PT.

heating rate of $5 \text{ }^\circ\text{C min}^{-1}$ and allowed to naturally cool to room temperature.

After CdS/Au/Ti/PMN-PT was obtained, the polarization of PMN-PT was carried out by switching ferroelectric domains [42]. Since PMN-

PT is a typical relaxation ferroelectrics, the dynamics of ferroelectric domains switching over PMN-PT can be detected via strain vs. electric field (S-E) curves [42,50]. The measurement configuration of polarization switching and S-E curves are shown in Fig. S1A. The strain measurements were performed using a four-probe method to monitor the resistances of two strain sensors (to detect the evolution of strain at [01–1] and [100] directions) with two Keithley 2400 source meters and using a two-probe with a Keithley 2410-C to apply electric field on PMN-PT substrates. The operation was controlled by Labview. The intrinsic PMN-PT displays eight directions (marked as R_1^+ / R_1^- , R_2^+ / R_2^- , R_3^+ / R_3^- , R_4^+ / R_4^- , in Fig. S1.B) of ferroelectric domains at random before polarizing, while the upward and downward self-polarization switching were revealed by S-E measurements (Fig. S1.C). When applying positive/negative electric field on the bottom/top of Au/Ti/PMN-PT, all the directions of ferroelectric domains will switch to the down/up direction, which induced an instantaneous large current. When the electric field is more than $\pm 1.6 \text{ kV cm}^{-1}$, the strain on the [100] will change from the tensile stress to the compressive stress then return the tensile stress because of the domain R_1^+ / R_1^- and R_2^+ / R_2^- switching each other.

2.2. Characterization

X-ray diffraction (XRD) patterns were recorded on an X'Pert MPD Pro X-ray diffractometer with $\text{Cu K}\alpha$ radiation at a scan rate of 0.05°s^{-1} at 2θ angle between 10° and 80° . UV-vis diffuse reflectance spectra (UV-vis DRS) were measured on a UV-vis spectrometer (SolidSpec DUC-3700). Scanning electron microscopy (SEM) and energy dispersive X-ray fluorescence spectroscopy (EDX) images were acquired using GeminiSEM 500. X-ray photoelectron spectra (XPS) were acquired in the Catalysis and Surface Science Endstation at the BL11U beamline in the National Synchrotron Radiation Laboratory at University of Science and Technology of China. Briefly, the beamline is connected to an undulator and equipped with two gratings that offer X-ray from 20 to 600 eV with a typical photon flux of $5 \times 10^{10} \text{ photons s}^{-1}$ and a resolution ($E/\Delta E$) better than 10^4 at 29 eV. The Fourier transform infrared spectra (FTIR) of the samples were obtained with a Nicolet iS50 spectrophotometer in the scan range of $800\text{--}4000 \text{ cm}^{-1}$. Raman spectra were recorded with a LabRamHR Raman microscope (J Y, France) under an excitation of 532 nm laser light. The transient infrared absorption signals were recorded on the Nicolet 870 FTIR spectrometer with the MCT detector. The synchronization between laser excitation and data acquisition was achieved with a Stanford Research Model DG535 pulse generator. In general, the lifetime of charge carriers depends on two tandem processes, that is, the relaxation process from instant excited state to the trap state and the subsequent exciton

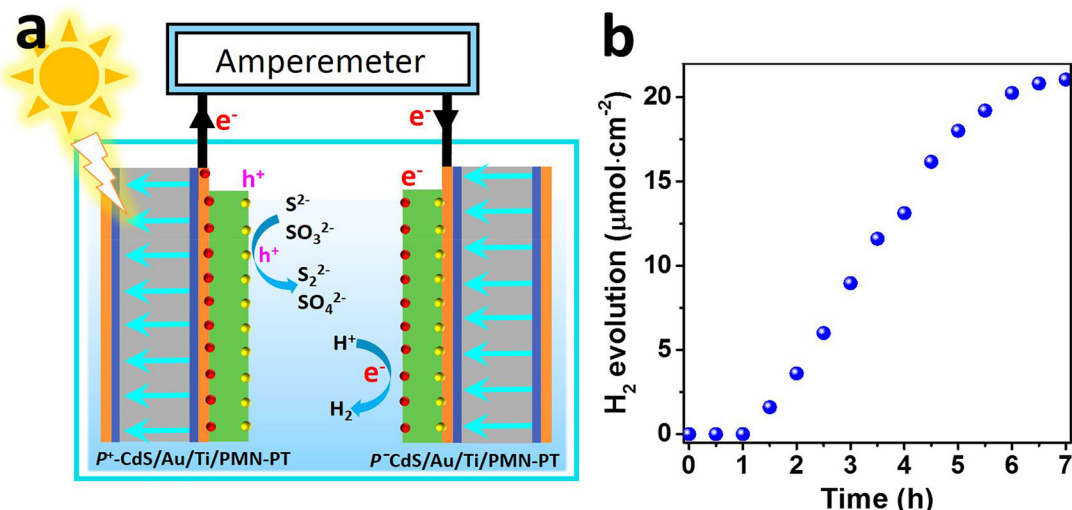


Fig. 9. (a) Scheme of a biphotovoltaic cell composed of P^+ -CdS/Au/Ti/PMN-PT and P^- -CdS/Au/Ti/PMN-PT without external bias voltage for photocatalytic water splitting. (b) H_2 evolution and STH curves over the biphotovoltaic cell without any bias under simulated sunlight (AM 1.5 G).

recombination process from the trap state to the ground state.

2.3. Photocatalytic activity measurements

The chronoamperometric responses of CdS/Au/Ti/PMN-PT without any externally applied voltage were measured on the two-electrode system, in which CdS/Au/Ti/PMN-PT electrode and platinum (Pt) electrode connected with an electric wire and covered with epoxy resin were placed in the two electrodes sites. As is known, S^{2-} in CdS is easy to be oxidized by photogenerated holes during the photocatalytic reaction [4]. In other words, self-oxidation by photogenerated holes (*i.e.* photocorrosion) still remains an issue for CdS. Taking this into consideration, the hole scavenger such as S^{2-} and SO_3^{2-} are usually used to suppress the photocorrosion [4]. Therefore in this study, the reaction was carried out in an aqueous solution (50 mL) of Na_2S (0.25 M) and Na_2SO_3 (0.35 M), pH = 12.5. The available electrode area immersed in the electrolyte solution was fixed to $0.5 \times 0.5 \text{ cm}^2$. During the photocatalytic reaction, the electrolyte solution was stirred while bubbling Ar. A Keitheiely 2410-C source meter recorder was used to detect the current of the system. In the terms of the biphotovoltaic cell composed of a positively and a negatively polarized CdS/Au/Ti/PMN-PT, the Pt electrode was replaced with one of the polarized CdS/Au/Ti/PMN-PT.

For the measurements with external applied voltage, the current vs. potential curves were obtained on a electrochemical workstation (CHI650E, CH Instrument Inc., Shanghai) using a three-electrode system with Ag/AgCl and Pt electrodes as reference and counter electrode, respectively. A 0.25 M Na_2S and 0.35 M Na_2SO_3 mixed aqueous solution (50 mL) was used as an electrolyte solution ($\text{pH} = 12.5$). The available electrode area immersed in the electrolyte solution was fixed to $0.5 \times 0.5 \text{ cm}^2$. The reactor was purged with Ar and maintained at atmospheric pressure. Photocurrent-time ($i-t$) curves were acquired under the chopped light irradiation with on/off interval of 10 s with a scan rate of 10 mV s^{-1} at an applied potential of 0.3 V, 0.9 V vs. reversible hydrogen electrode (RHE). Potentials referred to the Ag/AgCl electrode were converted to RHE using the Nernst equation as follows:

$$E_{(\text{vs. RHE})} = E_{(\text{vs. Ag/AgCl})} + E_{\text{Ag/AgCl (reference)}} + 0.0591 \text{ V} \times \text{pH}$$

where $E_{\text{Ag/AgCl (reference)}}$ is 0.1976 V with standard potential of the KCl-saturated Ag/AgCl electrode at 25 °C.

For the measurements of H_2 production, it was quantified on an online gas chromatograph (GC2014C, Shimadzu) using a thermal conductivity detector, a 5 Å molecular sieve column, and Ar as the carrier

gas. All the tests mentioned above were carried out under simulated sunlight (AM 1.5 G SAN-EI Electric Co., Ltd, XES-40S2-CE).

2.4. STH measurements

The STH values over CdS/Au/Ti/PMN-PT photocatalyst and biphotovoltaic cell without applied bias were assessed using the same experimental apparatus mentioned above. It was calculated by the equation,

$$\text{STH (\%)} = (R(H_2) \times \Delta G) / (P \times S) \times 100,$$

where $R(H_2)$, ΔG , P , and S are the rate of hydrogen evolution from the biphotovoltaic cell water splitting system, the change in Gibbs free energy that accompanies water splitting, the energy intensity of the solar light irradiation, and the effective irradiation area, respectively. The value of ΔG was 226 kJ mol^{-1} at 15°C .

3. Results and discussion

The configuration of CdS/Au/Ti/PMN-PT photocatalyst is shown Fig. 1. The typical ferroelectric $Pb(Mg_{1/3}Nb_{2/3})_{0.7}Ti_{0.3}O_3$ (PMN-PT) single crystal which exhibits the best performance on dielectric effect is used as the SPE layer to generate a nonvolatile polarization field [42]. The Ti layer deposited between the conductive Au layer and the PMN-PT substrates acts as an adhesive layer. The CdS photocatalyst is grown on the Au layer by a chemical bath method. The substrate PMN-PT displays eight directions of random ferroelectric domains before the polarization (shown in Fig. 1a middle scheme, and denoted as P^0 -CdS/Au/Ti/PMN-PT). These directions of domains could reorientate under bias, which leads to a single domain [42]. When a positive polarization of Au/Ti/PMN-PT takes place (Fig. 1a up scheme), all the directions of the ferroelectric domains could switch to the down direction, as shown in Fig. 1b, (marked as positive polarization, P^+ -CdS/Au/Ti/PMN-PT), and vice versa for negative polarization denoted as P^- -CdS/Au/Ti/PMN-PT (Fig. 1a down scheme and Fig. 1c). The polarization switching process is shown in Fig. S1 in the Supporting Information. In case that the P^+ -CdS/Au/Ti/PMN-PT is irradiated, the photons with energy higher than the band-gap of CdS could be absorbed by CdS to generate electrons and holes. In the photocatalytic reaction scheme (Fig. 1d), the photogenerated electrons in such P^+ -CdS/Au/Ti/PMN-PT system could directly migrate to the Au layer with the effect of SPE, and then transfer through an external wire to the platinum electrode to undergo H_2 production, leaving the photogenerated holes on the CdS side to

proceed the oxidation reaction with the sacrificial reagents of Na_2S and Na_2SO_3 .

The wurtzite CdS was obtained over Au/Ti/PMN-PT as indicated in XRD patterns (Fig. 2). The main peaks at 26.6° , 43.9° , and 52.0° are attributed to the diffraction of the (002), (110) and (112) of CdS (JCS Card: 41-1049) [51]. The composition of the as-obtained CdS/Au/Ti/PMN-PT is further supported by the high-resolution XPS, FTIR and Raman spectra. The difference between the binding energies of Cd 3d5/2 (405.1 eV) and Cd 3d3/2 (411.9 eV) peaks indicates Cd^{2+} states in CdS, while the S 2p peaks at 161.4 eV and 162.5 eV demonstrates S^{2-} in the CdS layer (Fig. 3) [52]. From the FTIR spectrum (Fig. S2.A), the typical characteristic absorption bands at 1121 cm^{-1} , 1042 cm^{-1} and 719 cm^{-1} are due to the vibrations of Cd–S bond in CdS [53–56]. The broad band centered at 3367 cm^{-1} and the band at 1633 cm^{-1} are contributed to by the surface adsorption of water molecules [57]. The intense and broad peaks in Raman spectrum (Fig. S2.B) at approximately 300, 600, and 900 cm^{-1} are assigned to fundamental optical phonon mode (1LO), the first over tone mode (2LO), and the second overtone (3LO) of CdS, respectively. These are in agreement with previous reports [58,59].

As observed from the cross-sectional SEM (Fig. 4a) and the corresponding EDX line scan (Fig. 4b) and mapping images (Fig. 4c–f), the morphology of the sample shows the expected layered structure of the CdS/Au/Ti/PMN-PT photocatalyst as illustrated in Fig. 1a. The uniform CdS layer with a thickness of 140 nm approximately can be controlled by the duration of the chemical bath reaction (Fig. S3). It can be estimated from the cross-sectional SEM (Fig. 4a) and the EDX line scan (Fig. 4b) that the conductive Au layer is about 20 nm. The thickness of the Au layer can also be controlled by the deposition time with a growth rate of *ca.* 0.2 \AA s^{-1} . The Au layer offers a direct pathway for the transportation of separated photogenerated electrons of CdS on the Au side, and thus improve the charge injection efficiency and collection efficiency [60–62]. Although Ti layer used as an adhesive layer for Au layer is too thin to be observed from the SEM image, it can be estimated as 5 nm via the EDX line scan.

Photocatalytic performances of CdS/Au/Ti/PMN-PT samples were evaluated under simulated sunlight in the absence of external bias conditions. As shown in Fig. 5, it can be seen that the photocurrent of P^+ -CdS/Au/Ti/PMN-PT yields $1.70\text{ mA}\cdot\text{cm}^{-2}$, which is about 20 times higher than that over P^- -CdS/Au/Ti/PMN-PT sample. This can be attributed to the SPE effect which promotes the separation of photo-generated carriers [33,34]. Importantly, the photocurrent of P^- -CdS/Au/Ti/PMN-PT is negligible, which indicates that the charge separation over the PMN-PT with random ferroelectric domains random is insufficient. In other words, the ferroelectric polarization in single domain induced charge separation is effectively achieved over P^+ -CdS/Au/Ti/PMN-PT. A negative photocurrent is observed over the P^- -CdS/Au/Ti/PMN-PT sample, because of the inverse electric field induced by the negative polarization. As such, the oxidation of S^{2-} and SO_3^{2-} occurs on the platinum electrode, while photogenerated electrons on the CdS side proceed the H_2 evolution. Therefore the absolute value of P^- -CdS/Au/Ti/PMN-PT lower than P^+ -CdS/Au/Ti/PMN-PT is possibly due to the slow kinetics of H_2 evolution on the surface of CdS in contrast to S^{2-} and SO_3^{2-} oxidation into S_2^{2-} and SO_4^{2-} . It should be pointed out that the photocurrent value of P^+ -CdS/Au/Ti/PMN-PT is sensitive to the thickness of CdS (Fig. S4). Obviously, a thick CdS benefits the adequate absorption of incident light, while goes against the effect of SPE as well as the long path for carrier transportation.

Moreover, the separation of charge carriers depends on the polarization-switching of PMN-PT (Fig. 6a). Once the positive polarization-switching was achieved, the photocurrent of P^+ -CdS/Au/Ti/PMN-PT remained unchanged (Fig. 6b). Notably, the directions of domains reorientate to a single domain when the voltages applied corresponds to or exceed the critical value of $+1.6\text{ kV}\text{ cm}^{-1}$ and $-1.6\text{ kV}\text{ cm}^{-1}$, respectively for positive and negative polarization-switching of PMN-PT. Taking advantages of the desirable strength of the SPE, the charge

separation could readily realized. However, the performance of P^+ -CdS/Au/Ti/PMN-PT is still lower than the maximum *ca.* $10.4\text{ mA}\text{ cm}^{-2}$ based on the band-gap of CdS (2.2 eV) (Fig. S5). This might be attributed to that the transport of separated electrons from the bulk of CdS to the conductive Au layer is limited by the unfavorable interface resistance, because the growth of CdS on Au/Ti/PMN-PT is not an epitaxial process.

Likewise, P^+ -CdS/Au/Ti/PMN-PT shows remarkable increase of H_2 evolution in comparison to P^- -CdS/Au/Ti/PMN-PT (Fig. 7), further demonstrating the enhancement of charge separation due to the SPE effect. According to the time-resolved infrared spectra of the sample (Fig. 8), the P^+ -CdS/Au/Ti/PMN-PT exhibits a prolonged lifetime of carriers in comparison to the non-polarized sample. The prolonged lifetime undoubtedly originates from the charge separation with SPE effect. Interestingly, the lifetime of charge carriers over P^+ -CdS/Au/Ti/PMN-PT sample is long enough to overcome the fast recombination according to the fitting results (Fig. S6). It can be seen that the H_2 evolved with a stable rate of $30\text{ }\mu\text{mol}\cdot\text{cm}^{-2}\text{ h}^{-1}$ in a hole sacrificial reagent circumstance. However, the H_2 evolution is about half less than the expected H_2 production calculated from the photocurrent of Fig. 5. It implies that the kinetics of water splitting in this study is dominated by the surface reaction between photogenerated carriers and reactants rather than the charge separation process [63]. The employment of cocatalyst strategy may harvest higher gas evolution, by fully taking advantage of the ability of carrier separation with the SPE effect [3,4,19]. With regard to the performances of CdS/Au/Ti/PMN-PT-based samples under an applied bias, the tendency was strongly correlated to that without bias (Fig. S7). This observation is in agreement with the study on ferroelectric polarization-enhanced photoelectrochemical water splitting [38]. In other words, the construction of photocatalysts with spontaneous polarization-induced charge separation is capable of enhancing the photocatalytic performance for both photocatalytic and photoelectrochemical systems.

Having confirmed the charge separation properties of samples with different polarization directions, it is reasonable to construct a bi-photoelectrode cell composed of a P^+ -CdS/Au/Ti/PMN-PT and a P^- -CdS/Au/Ti/PMN-PT as illustrated in Fig. 9a. In this case, the photogenerated electrons on P^+ -CdS/Au/Ti/PMN-PT could transfer to the Au side of P^- -CdS/Au/Ti/PMN-PT to recombine with photogenerated holes from P^- -CdS/Au/Ti/PMN-PT. Simultaneously, the photogenerated holes on the CdS side of P^+ -CdS/Au/Ti/PMN-PT could proceed the oxidation reaction with the sacrificial reagents of Na_2S or Na_2SO_3 and photogenerated electrons on the CdS side of P^- -CdS/Au/Ti/PMN-PT could reduce H_2O to evolve H_2 . It can be seen that the H_2 evolved with a rate of about $0.4\text{ }\mu\text{mol}\cdot\text{cm}^{-2}\text{ h}^{-1}$ (Fig. 9b). The initial evolution is negligible because the small amount of H_2 production is lower than the detection limit of the gas chromatograph. The apparent decrease is observed after 6 h, implying the insufficient durability of CdS in a long run even in a hole sacrificial reagent circumstance. The possible reason is that the kinetics of water splitting in this study is dominated by the surface reaction between photogenerated carriers and reactants. As a result, the unexpected accumulation of photogenerated holes on CdS/Au/Ti/PMN-PT corrode the CdS by oxidizing S^{2-} in CdS [43,64]. Therefore the surface reaction kinetics rather than the efficiency of charge separation is the main factor limiting the water splitting in this study. The STH can be calculated to be 0.19% during the stable stage. This value is considerable because of the unemployment of any noble metal cocatalysts or external bias. Furthermore, the successful construction of this bi-photoelectrode cell reflects the potential of the spontaneous polarization induced materials as a photoelectrodes replacing noble metal electrodes. In the proof of principle study, TiO_2 was used to fabricate $\text{TiO}_2/\text{Au}/\text{Ti}/\text{PMN-PT}$ via a pulse laser deposition method (Fig. S8). In such case, the interface resistance was lowered due to the epitaxial growth of TiO_2 . The example of $\text{TiO}_2/\text{Au}/\text{Ti}/\text{PMN-PT}$ demonstrated the universality of our fabrication method. In addition, it further confirmed that the efficiency of charge separation of samples with ferroelectric

polarization in a single domain is much higher than that in random domains.

4. Conclusions

The effective charge separation has been achieved via the development of a photocatalyst based on a ferroelectric polarization electric field with a single domain. CdS/Au/Ti/PMN-PT with positive SPE effect has reached a benchmark photocurrent of $1.70 \text{ mA}\cdot\text{cm}^{-2}$ for CdS without any applied bias. The first example of biphotoelectrode cell based on polarization-assisted electrodes was built, in tandem with a positively and a negatively polarized sample. It yield a STH of 0.19% which is considerable in reported biphotoelectrode cells without bias. The surface reaction kinetics rather than the efficiency of charge separation was found to be the factor limiting the water splitting. The present photocatalytic performance may be further enhanced through utilizing the cocatalyst strategy to accelerate the surface reaction and employing long wavelength-responsive materials. This work not only offers a facile method to generate SPE-induced carrier separation for efficient water splitting without any cocatalyst or external bias voltage but it also provides new insight into the potential application of polarization in biphotoelectrode cells.

Acknowledgements

This work was supported by National Key Research and Development Program of China (No. 2016YFB0700205), National Natural Science Foundation of China (U1632273, 21673214), Foundation from Key Laboratory of Photovoltaic and Energy Conservation, CAS (PECL2018KF012), Hefei Center for Physical Science and Technology (2016FXZY002), and Anhui Provincial Natural Science Foundation (17080885MB46). The authors thank the staff at BL11U beamline in NSRL for their assistance in acquiring XPS data.

Appendix A. Supplementary data

Supplementary material related to this article can be found, in the online version, at doi:<https://doi.org/10.1016/j.apcatb.2018.07.033>.

References

- [1] N. Lewis, *Science* 351 (2016) aad1920.
- [2] M. Grätzel, *Nature* 414 (2001) 338–344.
- [3] T. Hisatomi, J. Kubota, K. Domen, *Chem. Soc. Rev.* 43 (2014) 7520–7535.
- [4] A. Kudo, Y. Misaki, *Chem. Soc. Rev.* 38 (2009) 253–278.
- [5] S. Chen, T. Takata, K. Domen, *Nat. Rev. Mater.* 2 (2017) 17050.
- [6] B. Pinaud, J. Benck, L. Seitz, A. Forman, Z. Chen, T. Deutsch, B. James, K. Baum, G. Baum, S. Ardo, H. Wang, E. Miller, T. Jaramillo, *Energy Environ. Sci.* 6 (2013) 1983–2002.
- [7] J. Montoya, L. Seitz, P. Chakthanont, A. Vojvodic, T. Jaramillo, J. Nørskov, *Nat. Mater.* 16 (2016) 70–81.
- [8] J. Schneider, M. Matsouka, M. Takeuchi, J. Zhang, Y. Horiuchi, M. Anpo, D. Bahnemann, *Chem. Rev.* 114 (2014) 9919–9986.
- [9] L. Liu, L. Ding, Y. Liu, W. An, S. Lin, Y. Liang, W. Cui, *Appl. Catal. B* 201 (2017) 92–104.
- [10] J. Li, L. Cai, J. Shang, Y. Yu, L. Zhang, *Adv. Mater.* 28 (2016) 4059–4064.
- [11] A. Kubacka, M. Fernández-García, G. Colón, *Chem. Rev.* 112 (2012) 1555–1614.
- [12] J. Zhang, *J. Phys. Chem. B* 104 (2000) 7239–7253.
- [13] H. Tong, S. Ouyang, Y. Bi, N. Umezawa, M. Oshikiri, J. Ye, *Adv. Mater.* 24 (2012) 229–251.
- [14] M. Wang, H. Wang, Q. Wu, C. Zhang, S. Xue, *Int. J. Hydrogen Energy* 41 (2016) 6211–6219.
- [15] H. Wang, Y. Liang, L. Liu, J. Hu, W. Cui, J. Hazard. Mater. 344 (2018) 369–380.
- [16] X. Chen, L. Liu, P. Yu, S. Mao, *Science* 331 (2011) 746–750.
- [17] T. Kim, K. Choi, *Science* 343 (2014) 990–994.
- [18] X. Yu, N. Guijarro, M. Johnson, K. Sivula, *Nano Lett.* 18 (2018) 215–222.
- [19] J. Yang, D. Wang, H. Han, C. Li, *Acc. Chem. Res.* 46 (2013) 1900–1909.
- [20] S. Bai, W. Yin, L. Wang, Z. Li, Y. Xiong, *RSC Adv.* 6 (2016) 57446–57463.
- [21] K. Maeda, *ACS Catal.* 3 (2013) 1486–1503.
- [22] Q. Wang, T. Hisatomi, Q. Jia, H. Tokudome, M. Zhong, C. Wang, Z. Pan, T. Takata, M. Nakabayashi, N. Shibata, Y. Li, I. Sharp, A. Kudo, T. Yamada, K. Domen, *Nat. Mater.* 15 (2016) 611–615.
- [23] M. Zhu, Z. Sun, M. Fujitsuka, T. Majima, *Angew. Chem. Int. Ed.* 57 (2018) 2160–2164.
- [24] J. Low, J. Yu, M. Jaroniec, S. Wageh, A. Al-Ghamdi, *Adv. Mater.* 29 (2017) 1601694.
- [25] S. Ida, A. Takashiba, S. Koga, H. Hagiwara, T. Ishihara, *J. Am. Chem. Soc.* 136 (2014) 1872–1878.
- [26] L. Silva, S. Ryu, J. Choi, W. Choi, M. Hoffmann, *J. Phys. Chem. C* 112 (2008) 12069–12073.
- [27] Z. Ai, G. Zhao, Y. Zhong, Y. Shao, B. Huang, Y. Wu, *Appl. Catal. B* 221 (2018) 179–186.
- [28] Z. Wang, D. Cao, L. Wen, R. Xu, M. Obergfell, Y. Mi, Z. Zhan, N. Nasori, J. Demsar, Y. Lei, *Nat. Commun.* 7 (2016) 10348.
- [29] J. Zhu, S. Pang, T. Dittrich, Y. Gao, W. Nie, J. Cui, R. Chen, H. An, F. Fan, C. Li, *Nano Lett.* 17 (2017) 6735–6741.
- [30] N. Ma, K. Zhang, Y. Yang, *Adv. Mater.* 29 (2017) 1703694.
- [31] H. Li, Y. Sang, S. Chang, X. Huang, Y. Zhang, R. Yang, H. Jiang, H. Liu, Z. Wang, *Nano Lett.* 15 (2015) 2372–2379.
- [32] L. Li, P. Salvador, G. Rohrer, *Nanoscale* 6 (2014) 24–42.
- [33] A. Kakekhani, S. Ismail-Beigi, *ACS Catal.* 5 (2015) 4537–4545.
- [34] S. Nassreddine, F. Morfin, G. Niu, B. Vilquin, F. Gaillard, L. Piccolo, *Surf. Interface Anal.* 46 (2014) 721–725.
- [35] Y. Cui, J. Briscoe, S. Dunn, *Chem. Mater.* 25 (2013) 4215–4223.
- [36] H. Huang, S. Tu, C. Zeng, T. Zhang, A. Reshak, Y. Zhang, *Angew. Chem. Int. Ed.* 129 (2017) 11860–11864.
- [37] X. Zhang, M. Yates, *ACS Appl. Mater. Interfaces* 10 (2018) 17232–17239.
- [38] W. Yang, Y. Yu, M. Starr, X. Yin, Z. Li, A. Kvit, S. Wang, P. Zhao, X. Wang, *Nano Lett.* 15 (2015) 7574–7580.
- [39] Y. Cui, J. Briscoe, Y. Wang, N. Tarakina, S. Dunn, *ACS Appl. Mater. Interfaces* 9 (2017) 24518–24526.
- [40] W. Li, F. Wang, M. Li, X. Chen, Z. Ren, H. Tian, X. Li, Y. Lu, G. Han, *Nano Energy* 45 (2018) 304–310.
- [41] X. Huang, K. Wang, Y. Wang, B. Wang, L. Zhang, F. Gao, Y. Zhao, W. Feng, S. Zhang, P. Liu, *Appl. Catal. B* 227 (2018) 322–329.
- [42] H. Fu, R. Coben, *Nature* 403 (2000) 281–283.
- [43] T. Simon, N. Bouchonville, M. Berr, A. Vaneski, A. Adrović, D. Volbers, R. Wyrywich, M. Döblinger, A. Susha, A. Rogach, F. Jäckel, J. Stolarsky, J. Feldmann, *Nat. Commun.* 13 (2014) 1013–1018.
- [44] K. Wu, H. Zhu, Z. Liu, W. Rodríguez-Córdoba, T. Lian, *J. Am. Chem. Soc.* 134 (2012) 10337–10340.
- [45] X. Zheng, J. Song, T. Ling, Z. Hu, P. Yin, K. Davey, X. Du, S. Qiao, *Adv. Mater.* 28 (2016) 4935–4942.
- [46] M. Todeschini, A. Bastos da Silva Fanta, F. Jensen, J. Wagner, A. Han, *ACS Appl. Mater. Interfaces* 9 (2017) 37374–37385.
- [47] B. Hong, Y. Yang, J. Zhao, K. Hu, J. Peng, H. Zhang, W. Liu, Z. Luo, H. Huang, X. Li, C. Gao, *Mater. Lett.* 169 (2016) 110–113.
- [48] W. Septina, S. Gunawan, T. Ikeda, M. Harada, R. Higashi, M. Abe, Matsumura, *J. Phys. Chem. C* 119 (2015) 8576–8583.
- [49] L. Cheng, Q. Xiang, Y. Liao, H. Zhang, *Energy Environ. Sci.* 11 (2018) 1362–1391.
- [50] S. Dunn, D. Tiwari, P. Jones, D. Gallardo, *J. Mater. Chem.* 17 (2007) 4460–4463.
- [51] W. Chen, X. Ning, B. Yang, Y. Wu, Z. Li, G. Lu, *Appl. Catal. B* 221 (2018) 243–257.
- [52] J. Zhang, W. Li, Y. Li, L. Zhong, C. Xu, *Appl. Catal. B* 217 (2017) 30–36.
- [53] R. Lakshminpathy, N. Sarada, K. Chidambaram, S. Pasha, *Int. J. Nanomed.* 10 (2015) 183–188.
- [54] S. Mali, S. Desai, D. Dalavi, C. Betty, P. Bhosale, P. Patil, *Photochem. Photobiol. Sci.* 10 (2011) 1652–1658.
- [55] F. Jiang, T. Yan, H. Chen, A. Sun, C. Xu, X. Wang, *Appl. Surf. Sci.* 295 (2014) 164–172.
- [56] L. Ge, F. Zuo, J. Liu, Q. Ma, C. Wang, D. Sun, L. Bartels, P. Feng, *J. Phys. Chem. C* 116 (2012) 13708–13714.
- [57] J. Fu, B. Chang, Y. Tian, F. Xi, X. Dong, *J. Mater. Chem. A* 1 (2013) 3083–3090.
- [58] X. Wu, J. Zhao, L. Wang, M. Han, M. Zhang, H. Wang, H. Huang, Y. Liu, Z. Kang, *Appl. Catal. B* 207 (2017) 501–509.
- [59] D. Chu, C. Dai, W. Hsieh, C. Tsai, *J. Appl. Phys.* 69 (1991) 8402–8404.
- [60] Z. Li, W. Luo, M. Zhang, J. Feng, Z. Zou, *Energy Environ. Sci.* 6 (2013) 347–370.
- [61] M. Walter, E. Warren, J. McKone, S. Boettcher, Q. Mi, E. Santori, N. Lewis, *Chem. Rev.* 110 (2010) 6446–6473.
- [62] K. Sivula, R. van de Krol, *Nat. Rev. Mater.* 1 (2016) 15010.
- [63] F. Osterloh, *Chem. Soc. Rev.* 42 (2014) 2294–2320.
- [64] Q. Li, X. Li, S. Wageh, A. Al-Ghamdi, J. Yu, *Adv. Energy Mater.* 5 (2015) 1500010.